RSC Advances

PAPER

View Article Online
View Journal | View Issue

Cite this: *RSC Adv.*, 2015, **5**, 73077

Preparation, crystal structure and up-conversion luminescence of Er^{3+}, Yb^{3+} co-doped $Gd_2(WO_4)_3$

Mengyan Yin,[a] Yangai Liu,*[a] Lefu Mei,*[a] Maxim S. Molokeev,[b] Zhaohui Huang[a] and Minghao Fang[a]

Received 3rd July 2015
Accepted 17th August 2015

DOI: 10.1039/c5ra12959a

www.rsc.org/advances

Up-conversion (UC) phosphors $Gd_2(WO_4)_3$:Er^{3+}/Yb^{3+} were synthesized by a high temperature solid-state reaction method. The crystal structure of $Gd_2(WO_4)_3$:3% Er^{3+}/10% Yb^{3+} was refined by Rietveld method and it was showed that Er^{3+}/Yb^{3+} were successfully doped into the host lattice replacing Gd^{3+}. Under 980 nm laser excitation, intense green and weak red emissions centered at around 532 nm, 553 nm, and 669 nm were observed, which were assigned to the Er^{3+} ion transitions of $^4H_{11/2} \rightarrow {}^4I_{15/2}$, $^4S_{3/2} \rightarrow {}^4I_{15/2}$ and $^4F_{9/2} \rightarrow {}^4I_{15/2}$, respectively. The optimum Er^{3+} doping concentration was determined as 3 mol% when the Yb^{3+} concentration was fixed at 10 mol%. The pump power study indicated that the energy transfer from Yb^{3+} to Er^{3+} in Er^{3+}, Yb^{3+} co-doped $Gd_2(WO_4)_3$ was a two-photon process, and the related UC mechanism of energy transfer was discussed in detail.

Introduction

Near-Infrared-to-visible (NIR) up-conversion is an optical process, when near infrared photons are converted into visible photons by multiphoton absorption, which is governed with the anti-Stokes rule.[1,2] The UC luminescence has attracted a lot of interest from researchers because of its wide potential applications, such as bio-labels, solar cells, optical data storage, displays and so on.[3–9] For UC phosphors, excellent fluorescence is always achieved by doping rare earth (RE) ions into luminescent hosts. Among various ions, Er^{3+} is the one of the most studied active ions. Since Er^{3+} has a long life of intermediates level and abundant 4f level structure, it can continuously emit green or red photons when excited by high energy photons.[10] In contrast, Yb^{3+} ions are doped as a sensitizer, and it can enhance the near-infrared (around 980 nm) absorption and improve the UC luminescent efficiency of Er^{3+}.

The host matrixes play a crucial role in the UC process. The good hosts can support doped ions in a fine crystalline field, in which energy transfer (ET) can easily take place in the host, and, thus, improve significantly the luminescence properties. To be more specific, host materials should be chemically stable and have low phonon energy to avoid efficiency loss *via* non-radiative transfer.[11] Tungstate crystals are among classic inorganic luminescent materials.[12] In 1896, the X-ray luminescence of $CaWO_4$ was discovered by Pupin.[13] The tungstate crystals provide great mechanical strength and chemical and thermal stability.[14,15] Because of the strong covalent W–O bond in WO_4^{2-} groups, the tungstate can improve the averaged covalency of crystal, and, respectively, the solubility of rare earth ions can be enhanced.[16–19] Of those researches of tungstate doped with rare earth phosphors, most are single tungstate crystals similar to scheelite and double tungstate crystals $ALn(WO_4)_2$ (A = alkali metal ions, Ln = rare earth ions). While, there is less study on poly-tungstate.

Gadolinium tungstate, $Gd_2(WO_4)_3$, can be doped easily doped by Er^{3+}/Yb^{3+} at Gd^{3+} position because of the similar ionic radius and electrovalence of Gd^{3+} and Er^{3+}/Yb^{3+}. Besides, the ionic radius of Gd^{3+} is larger than that of Er^{3+} and Yb^{3+}, and it can be easily substituted by Er^{3+} and Yb^{3+}.[20,21] Li *et al.*[22] prepared Er^{3+}/Yb^{3+} co-doped $Gd_2(WO_4)_3$ *via* a co-precipitation method, and investigated pumping-route-dependent concentration quenching and temperature effect on the phosphors. Sun *et al.*[23] prepared Er^{3+}/Yb^{3+} co-doped $Gd_2(WO_4)_3$ and Gd_2WO_6 using co-precipitation method, and reported the up-converted emission differences between those two phosphors. However, the crystal structure of $Gd_2(WO_4)_3$ has not been reported, and how the doped ions affect the lattice parameters and structure of $Gd_2(WO_4)_3$ host has not been discussed.

In this research, Er^{3+}/Yb^{3+} co-doped $Gd_2(WO_4)_3$ phosphors have been synthesized by a conventional high temperature solid-state reaction method. The crystal structure of $Gd_2(WO_4)_3$:3% Er^{3+}/10% Yb^{3+} is refined by Rietveld method. And the structural characteristics and UC luminescent characteristics of phosphors are investigated. Also, the rare earth ion doping concentration effect on the UC luminescence and the UC mechanism of energy transfer are discussed.

[a]*School of Materials Science and Technology, Beijing Key Laboratory of Materials Utilization of Nonmetallic Minerals and Solid Wastes, National Laboratory of Mineral Materials, China University of Geosciences, Beijing 100083, China. E-mail: liuyang@cugb.edu.cn; mlf@cugb.edu.cn*

[b]*Laboratory of Crystal Physics, Kirensky Institute of Physics, SB RAS, Krasnoyarsk 660036, Russia*

Experimental

The $Gd_2(WO_4)_3$:$x$$Er^{3+}$/0.1$Yb^{3+}$ (x = 0, 0.001, 0.01, 0.02, 0.03, 0.04, 0.05) phosphors and $Gd_2(WO_4)_3$:0.03Er^{3+}/$y$$Yb^{3+}$ (y = 0, 0.05, 0.1, 0.015, 0.2, 0.025) phosphors were synthesized by the high temperature solid-state reaction method. The starting materials of Gd_2O_3 (99.99%), Er_2O_3 (99.99%), Yb_2O_3 (99.99%), and WO_3 (A.R.) were mixed based on stoichiometric ratio and ground in an agate mortar. The mixtures were reacted in an aluminum crucible at 1050 °C for 12 hours in resistance furnace in the air. After the furnace cooled down naturally, the samples were ground for further test.

The phase composition of as-prepared phosphors was examined by X-ray diffraction measurement (XRD, D8 Advance diffractometer, Bruker, Germany, with Cu-Kα and linear VANTEC detector, λ = 0.15406 nm, 40 kV, 30 mA). The powder diffraction data of $Gd_2(WO_4)_3$:3% Er^{3+}/10% Yb^{3+} for Rietveld analysis was collected at room temperature by the step size of 0.02° (2θ), and the counting time was 3 s per step. The Rietveld refinement was performed using package TOPAS 4.2.[24] The Fourier transform infrared spectrum (FT-IR) was recorded over the range of 4000–400 cm^{-1} by an Excalibur 3100 (USA) device. The diffuse reflection spectra were measured by UV-NIR spectrophotometer (Cary 5000, USA). The UC luminescence spectra were collected at room temperature with a Hitachi F-4600 spectrophotometer equipped with an external power-controllable 980 nm semiconductor laser (Beijing Viasho Technology Company, China) as the excitation source.

Results and discussion

The XRD patterns of the as-prepared pure $Gd_2(WO_4)_3$, $Gd_2(WO_4)_3$:Er^{3+}/Yb^{3+} and the standard PDF diffraction pattern of $Gd_2(WO_4)_3$ are shown in Fig. 1(a). All the diffraction peaks of the samples fitted well with the standard data of $Gd_2(WO_4)_3$ (JCPDS no. 23-1076), indicating that pure $Gd_2(WO_4)_3$ has been successfully synthesized by the high temperature solid-state reaction method at 1050 °C for 12 h. Besides, the Er^{3+} and Yb^{3+} cannot be detected, which shows that the Er^{3+} and Yb^{3+} are completely doped in the host lattice,[25] and did not change the crystal structure of $Gd_2(WO_4)_3$.[26,27] The measurement of the FT-IR spectra of pure $Gd_2(WO_4)_3$ is shown in Fig. 1(b). In pure $Gd_2(WO_4)_3$, the strong absorption peaks corresponding to the vibrations of WO_4^{2-} groups are between 400 and 1000 cm^{-1}. The absorption bands at around 734 and 837 cm^{-1} are related to O–W–O stretch vibrations of WO_4^{2-} tetrahedron.[28,29] The 418 and 460 cm^{-1} band can be attributed to the stretching vibration of W–O.[30]

The structure of $Gd_2(WO_4)_3$:3% Er^{3+}, 10% Yb^{3+} is unknown, and, for the Rietveld refinement, the XRD pattern is indexed by monoclinic cell ($C2/c$) with parameters close to those of $Eu_2(WO_4)_3$: (ICSD #15877).[31,32] The refinement is stable and gives low R-factors (Table 1, Fig. 2). The atom coordinates and main bond lengths are listed in Tables 2 and 3 respectively. The crystal structure of $Gd_2(WO_4)_3$:3% Er, 10% Yb is depicted in Fig. 3. As seen from Fig. 3, the coordination number of Gd^{3+} ions in $Gd_2(WO_4)_3$ is eight. The ionic radii of Gd^{3+}(CN = 8) = 1.053, while the ionic radii of dopants are IR(Yb^{3+}, CN = 8) = 0.985,

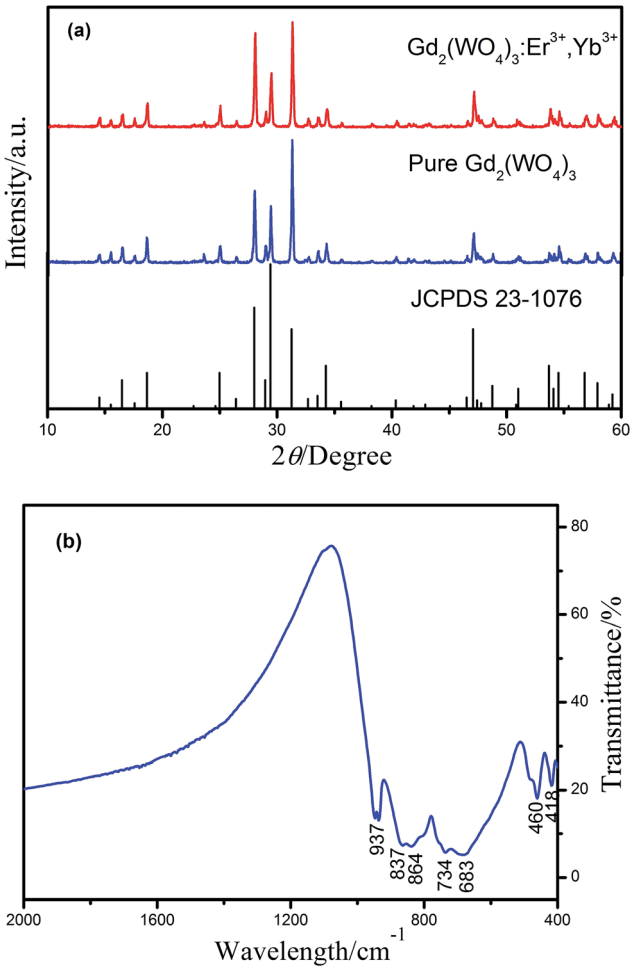

Fig. 1 (a) XRD patterns of $Gd_2(WO_4)_3$ and Er^{3+}/Yb^{3+} co-doped $Gd_2(WO_4)_3$ and the standard data of $Gd_2(WO_4)_3$ (JCPDS 23-1076) as a reference; (b) FT-IR spectra of pure $Gd_2(WO_4)_3$.

IR(Er^{3+}, CN = 8) = 1.004, which are smaller and closer than IR(Gd^{3+}, CN = 8).[33] Thus the Gd^{3+} ions are successfully replaced by Yb^{3+} and Er^{3+} ions, which should lead to the host cell parameters shrinkage. The crystallographic data and refinement parameters are shown in Table 1. The cell volume of $Gd_2(WO_4)_3$:Er^{3+}, Yb^{3+} is V = 936.65(5) Å^3, compared with the stand cell volume of $Gd_2(WO_4)_3$, V = 938.15 Å^3,[34] which indicates that the cell volume decrease on the doping by Er^{3+} and Yb^{3+}.

Table 1 Main parameters of processing and refinement of the $Gd_2(WO_4)_3$:3% Er, 10% Yb sample

Compound		$Gd_2(WO_4)_3$:3% Er, 10% Yb	
Sp. Gr.	$C2/c$	No. of reflections	492
a, Å	7.6541 (2)	No. of refined parameters	66
b, Å	11.4140 (3)	R_{wp}, %	12.66
c, Å	11.3909 (3)	R_p, %	8.67
β, °	109.744 (2)	R_{exp}, %	4.83
V, Å^3	936.65 (5)	χ^2	2.62
Z	1	R_B, %	3.35
2θ-interval, °	5–100		

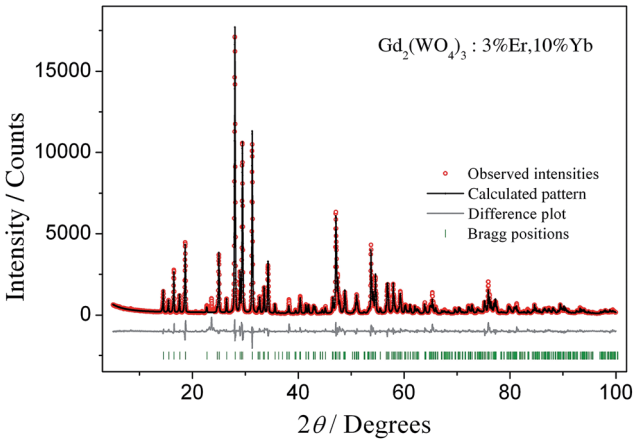

Fig. 2 Difference Rietveld plot of $Gd_2(WO_4)_3$:3% Er, 10% Yb.

Table 2 Fractional atomic coordinates and isotropic displacement parameters (Å^2) of $Gd_2(WO_4)_3$:3% Er, 10% Yb

Atom	*x*	*y*	*z*	B_{iso}	Occ.
Gd	0.3272 (10)	0.3786 (4)	0.4069 (4)	0.3 (3)	0.87
Yb1	0.3272 (10)	0.3786 (4)	0.4069 (4)	0.3 (3)	0.1
Er1	0.3272 (10)	0.3786 (4)	0.4069 (4)	0.3 (3)	0.03
W1	0	0.1327 (3)	0.25	0.6 (3)	1
W2	0.1536 (7)	0.3921 (2)	0.0516 (2)	0.3 (3)	1
O1	0.168 (6)	0.047 (2)	0.223 (4)	1.5 (5)	1
O2	0.126 (6)	0.212 (3)	0.384 (4)	1.5 (5)	1
O3	0.223 (6)	0.324 (3)	0.199 (3)	1.5 (5)	1
O4	0.366 (7)	0.449 (3)	0.040 (3)	1.5 (5)	1
O5	0.060 (7)	0.463 (3)	0.423 (4)	1.5 (5)	1
O6	0.442 (6)	0.210 (3)	0.060 (4)	1.5 (5)	1

Table 3 Main bond lengths (Å) of $Gd_2(WO_4)_3$:3% Er, 10% Yb[a]

(Gd, Yb, Er)–O1^{i}	2.43 (3)	W1–O1	1.72 (3)
(Gd, Yb, Er)–O2	2.40 (3)	W1–O2	1.75 (4)
(Gd, Yb, Er)–O2^{ii}	2.51 (4)	W2–O3	1.76 (3)
(Gd, Yb, Er)–O3	2.31 (4)	W2–O4	1.79 (4)
(Gd, Yb, Er)–O4^{iii}	2.36 (4)	W2–O5^{v}	1.93 (4)
(Gd, Yb, Er)–O4^{iv}	2.44 (3)	W2–O6^{vi}	1.70 (4)
(Gd, Yb, Er)–O5	2.33 (4)		
(Gd, Yb, Er)–O6^{iii}	2.56 (3)		

[a] Symmetry codes: (i) $-x+1/2, y+1/2, -z+1/2$; (ii) $-x+1/2, -y+1/2, -z+1$; (iii) $-x+1, y, -z+1/2$; (iv) $x, -y+1, z+1/2$; (v) $-x+1/2, y-1/2, -z+1/2$; (vi) $-x, y, -z+1/2$.

The diffuse reflection of pure $Gd_2(WO_4)_3$, Yb^{3+} doped $Gd_2(WO_4)_3$, Er^{3+} doped $Gd_2(WO_4)_3$ and Yb^{3+}/Er^{3+} co-doped $Gd_2(WO_4)_3$ are shown in Fig. 4. From the figure, pure $Gd_2(WO_4)_3$ does not show apparent absorption in the range of 300–1200 nm. The Er^{3+}-doped $Gd_2(WO_4)_3$ possesses strong absorption at 520, 655, 795 nm, while weak absorption at 974 nm is observed. The absorption at 974 nm originated from $^2F_{7/2} \rightarrow {}^2F_{5/2}$ transition of Yb^{3+} ions is observed in Yb^{3+}-doped $Gd_2(WO_4)_3$. Yb^{3+} and Er^{3+} co-doped $Gd_2(WO_4)_3$ sample is characterized by the apparent absorption at 520, 655, 795 and

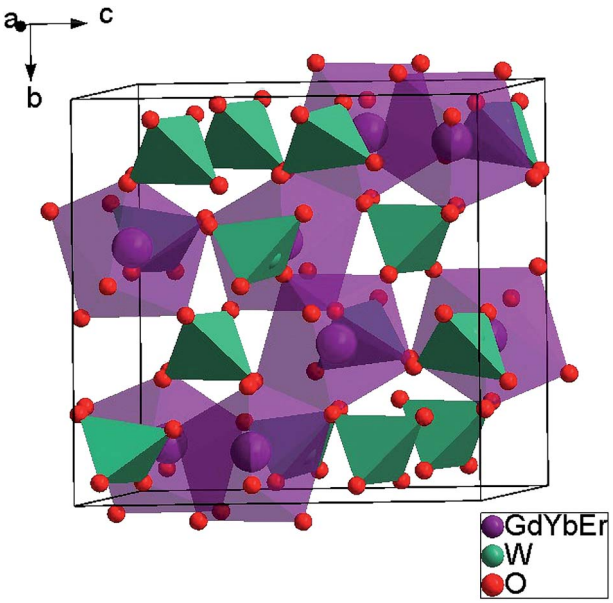

Fig. 3 The crystal structure of $Gd_2(WO_4)_3$:3% Er, 10% Yb.

974 nm. From the insets, it is obvious that Yb^{3+}/Er^{3+} co-doped $Gd_2(WO_4)_3$ exhibits higher UC efficiency than that of Er^{3+}-doped $Gd_2(WO_4)_3$, which demonstrates that the increasing absorption at 980 nm of Er^{3+} is mainly caused by the energy transition of Yb^{3+} to Er^{3+}.[35]

The UC luminescence spectra of single Yb^{3+} doped and $xEr^{3+}/0.1Yb^{3+}$ (x = 0–0.05) co-doped $Gd_2(WO_4)_3$ under 980 nm near-infrared laser excitation at room temperature is shown in Fig. 5, and the inset shows the dependence of green UC emission intensity (at 532 nm and 553 nm) on Er^{3+} concentration. First of all, Yb^{3+}-doped $Gd_2(WO_4)_3$ does not show the UC luminescence because of activator Er^{3+} ions absence. Due to concentration quenching effect,[36] UC luminescence green

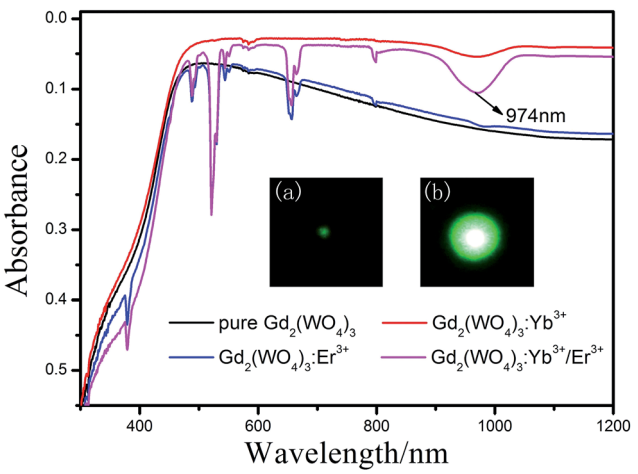

Fig. 4 Diffuse reflection spectra of pure $Gd_2(WO_4)_3$, Yb^{3+} doped $Gd_2(WO_4)_3$, Er^{3+} doped $Gd_2(WO_4)_3$ and Yb^{3+}/Er^{3+} co-doped $Gd_2(WO_4)_3$, and the inset shows the green luminescence images of the phosphors when irradiated by a 980 nm diode ((a) Er^{3+} doped $Gd_2(WO_4)_3$, (b) Yb^{3+}/Er^{3+} co-doped $Gd_2(WO_4)_3$).

emission intensities increase firstly and, then, decrease approaching the maximum at 3 mol% of Er^{3+} content (Yb^{3+} concentration was fixed at 10 mol%). In the spectra, two strong green emission bands centered at 532 nm and 553 nm and a weak red emission band centered at around 669 nm are observed, which are assigned to the Er^{3+} ion transitions of $^4H_{11/2} \rightarrow {}^4I_{15/2}$, $^4S_{3/2} \rightarrow {}^4I_{15/2}$ and $^4F_{9/2} \rightarrow {}^4I_{15/2}$, respectively.[20,35,37]

The UC luminescence spectra of single Er^{3+} doped and 0.03 Er^{3+}/$y$$Yb^{3+}$ ($y = 0$–0.25) co-doped $Gd_2(WO_4)_3$ under 980 nm near-infrared laser excitation are presented in Fig. 6, and the inset shows the variation of the UC luminescent intensity at 532 nm and 553 nm on the Yb^{3+} concentration increase. Similarly, when singly doped with Er^{3+} ion, the UC spectrum includes very weak UC emission, because Er^{3+} solely can hardly absorb the near-infrared excitation energy in the absence of sensitizer Yb^{3+} ions. With increasing concentration of Yb^{3+}, the UC emission regions are enhanced. Moreover, it is also found that the two strong green emission bands and one weak red emission band are assigned to the Er^{3+} ion transitions.

The UC mechanism can be explained by the dependence of UC emission intensity (I) on pump power (P), which follows the relation: $I \propto P^n$,[20,25,38] where n is the pump photon number required for the transition from ground state to upper emitting state. The number n is obtained from the slope of the fitting line of log I *versus* log P. Fig. 7 shows the UC luminescence spectrum of $Gd_2(WO_4)_3$:0.03Er^{3+}/0.1Yb^{3+} with different pump powers, and the double-logarithmic plot of green and red UC emission intensities upon pump powers is shown in the inset. It is obvious that the UC luminescence intensity of the phosphors increases as the pump power increased. The calculated slopes are 2.12, 2.12 for the green emission (532 nm: $^4H_{11/2} \rightarrow {}^4I_{15/2}$, 553 nm: $^4S_{3/2} \rightarrow {}^4I_{15/2}$), and 1.48 for the red emission (669 nm: $^4F_{9/2} \rightarrow {}^4I_{15/2}$), indicating that both green emission and red emission are two-photon process.[39–41]

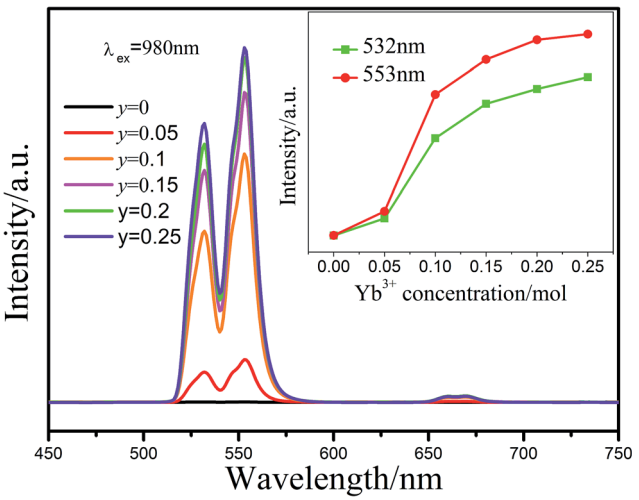

Fig. 6 Comparison of UC luminescence spectra of $Gd_2(WO_4)_3$:0.03-Er^{3+}/$y$$Yb^{3+}$ under 980 nm laser excitation. The inset shows the intensity of the green emission as a function of Yb^{3+} doping concentration.

The deviation from the theoretical value 2 for those special two-photon process may be caused by the crystal structure and the defect states inside the bandgap in the energy transition.[20,40] The n value lower than 2 for red emission at 669 nm could be due to the large UC rate for the depletion of the intermediate excited states, competition between linear decay, and the local thermal effect as well.[25] In the limit of infinitely small UC rates, the UC luminescence intensity for a special n-photon energy transfer tends to be proportional to n-th power of pump power (P^n); while in the limit of infinitely large UC rate, the intensity is proportional to the pump power (P^1). Thus, the UC intensity which excited by the sequential absorption of n photons has a dependence of P^β on pump power, with β ranges from 1 to n.[42] Besides, as the excitation power is increased, the slope may

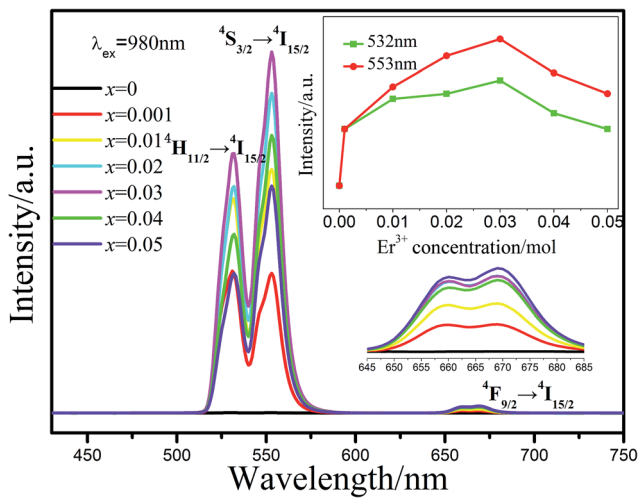

Fig. 5 Comparison of UC luminescence spectra of $Gd_2(WO_4)_3$:$x$$Er^{3+}$/0.1$Yb^{3+}$ under 980 nm laser excitation and the inset shows the intensity of the green emission as a function of Er^{3+} doping concentration and the enlarged red emission band.

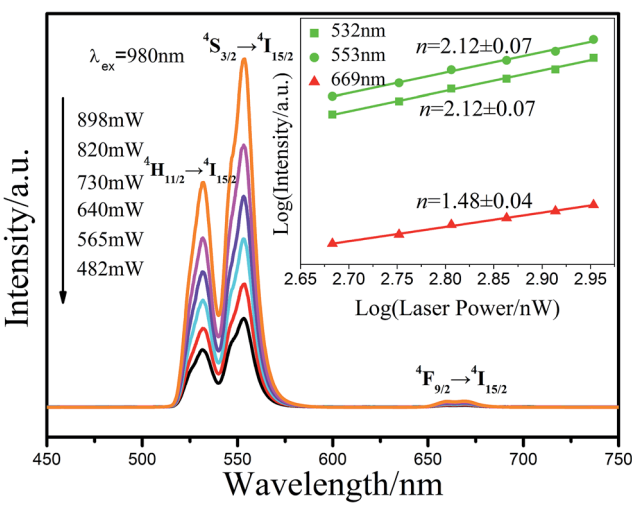

Fig. 7 UC emission spectra of $Gd_2(WO_4)_3$:0.03Er^{3+}/0.1Yb^{3+} with different pump power, and the inset shows the dependence of green and red UC emission intensities upon pump power.

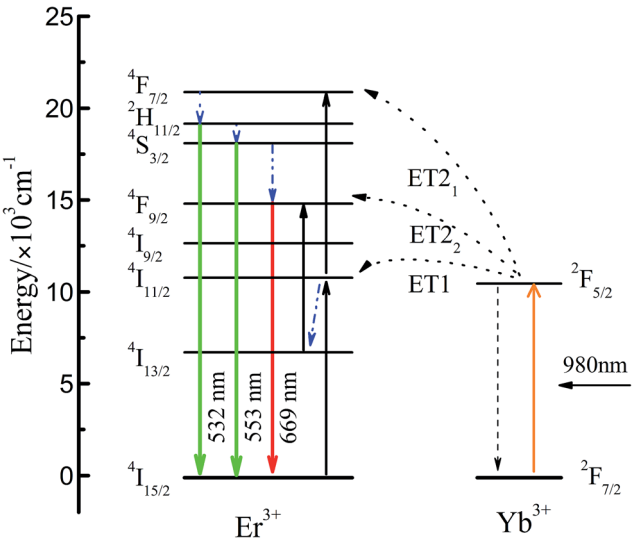

Fig. 8 The energy level diagrams of Er^{3+} and Yb^{3+} ions, and the proposed UC mechanism in $Gd_2(WO_4)_3$:Er^{3+}/Yb^{3+} phosphors.

decrease, which may due to the self-focusing,[43] or the high excitation densities may lead to high non-radiative rates and high temperature in the internal samples, and then, the thermal effect causes the quenching of UC intensity.[42]

According to the above results, the energy level diagram of the Er^{3+} and Yb^{3+} ions and the proposed UC mechanism in Er^{3+}/Yb^{3+} co-doped $Gd_2(WO_4)_3$ are illustrated in Fig. 8. Under the 980 nm excitation, Yb^{3+} ion can be excited by one photon and transferred from the ground state $^2F_{7/2}$ to the excited state $^2F_{5/2}$. The Er^{3+} ion may be excited and transferred from the ground state $^4I_{15/2}$ to the excited state $^4I_{11/2}$ through the ground state absorption (GSA), or may be excited though the energy transfer (ET1) from Yb^{3+} ion. The second step of $ET2_1$ can promote an excited state absorption (ESA) of Er^{3+} from $^4I_{11/2}$ to the $^4F_{7/2}$ level.[38]

Because of the small energy gap between the $^4F_{7/2}$, $^4H_{11/2}$ and $^4S_{3/2}$, the transition of Er^{3+} occurred rapidly from the $^4F_{7/2}$ to the $^4H_{11/2}$ and $^4S_{3/2}$ by non-radiative relaxation (NR).[35] Finally, the green emissions centered at 532 nm and 553 nm were produced through radiative transitions of $^4H_{11/2} \rightarrow {}^4I_{15/2}$ and $^4S_{3/2} \rightarrow {}^4I_{15/2}$. The red emission centered at 669 nm was associated with $^4F_{9/2} \rightarrow {}^4I_{15/2}$ due to the NR from $^4S_{3/2}$ to the $^4F_{9/2}$ level or the $ET2_2$: $^2F_{5/2}$ (Yb^{3+}) + $^4I_{13/2}$(Er^{3+}) $\rightarrow$ $^2F_{7/2}$(Yb^{3+}) + $^4F_{9/2}$(Er^{3+}).[29]

Conclusions

Er^{3+}, Yb^{3+} single-doped and Er^{3+}/Yb^{3+} co-doped $Gd_2(WO_4)_3$ phosphors were successfully synthesized by the high temperature solid-state method at 1050 °C for 12 h. The Er^{3+} and Yb^{3+} doping induced the lattice parameters decrease which proved the Gd^{3+} replacement by Er^{3+} and Yb^{3+} ions. Under the 980 nm laser excitation, the Er^{3+} or Yb^{3+} single-doped $Gd_2(WO_4)_3$ samples hardly show the UC luminescence. While the Er^{3+}/Yb^{3+} co-doped $Gd_2(WO_4)_3$ phosphors exhibited remarkable green UC emission at 532 and 553 nm and the low-intensity red UC emission at around 669 nm, which were assigned to the characteristic level transition of $^4H_{11/2} \rightarrow {}^4I_{15/2}$, $^4S_{3/2} \rightarrow {}^4I_{15/2}$ and $^4F_{9/2} \rightarrow {}^4I_{15/2}$ of Er^{3+} ion, respectively. The optimum Er^{3+} doping concentration was determined as 3 mol%. With the Yb^{3+} doping concentration increase, the UC emission intensities of Er^{3+}/Yb^{3+} co-doped $Gd_2(WO_4)_3$ enhanced gradually. The power-dependent luminescent properties indicated that the energy transfer existed in both green and red emissions was a two-photon process. Generally, the results of the present study demonstrates that the Er^{3+}/Yb^{3+} co-doped $Gd_2(WO_4)_3$ is an efficient green emission UC phosphor.

Acknowledgements

The present work was supported by the National Natural Science Foundations of China (Grant No. 51472223), the Fundamental Research Funds for the Central Universities (Grant No. 2652015008), and New Century Excellent Talents in University of Ministry of Education of China (Grant No. NCET-12-0951).

Notes and references

1 F. Auzel, *Chem. Rev.*, 2004, **104**, 139.
2 F. Wang and X. Liu, *Chem. Soc. Rev.*, 2009, **38**, 976–989.
3 L. Shi, C. Li, Q. Shen and Z. Qiu, *J. Alloys Compd.*, 2014, **591**, 105–109.
4 A. Patra, C. S. Friend, R. Kapoor and P. N. Prasad, *J. Phys. Chem. B*, 2002, **106**, 1909.
5 E. A. Ferreira, F. C. Cassanjes and G. Poirier, *Opt. Mater.*, 2013, **35**, 1141–1145.
6 K. Teshima, S. Lee, N. Shikine, T. Wakabayashi, K. Yubuta, T. Shishido and S. Oishi, *Cryst. Growth Des.*, 2011, **11**, 995–999.
7 A. Shalav, B. S. Richards and M. A. Green, *Sol. Energy Mater. Sol. Cells*, 2007, **91**, 829–842.
8 X. Li, D. Zhao and F. Zhang, *Theranostics*, 2013, **3**, 292–305.
9 C. Guo, J. Yu, J.-H. Jeong, Z. Ren and J. Bai, *Phys. B*, 2011, **406**, 916–920.
10 T. Li, C.-F. Guo, Y.-M. Yang, L. Li and N. Zhang, *Acta Mater.*, 2013, **61**, 7481–7487.
11 D. Vennerberg and Z. Lin, *Sci. Adv. Mater.*, 2011, **3**, 26–40.
12 Q.-H. Zeng, X.-G. Zhang, P. He, H.-B. Liang and M.-L. Gong, *J. Inorg. Organomet. Polym. Mater.*, 2010, **25**, 1009–1014.
13 G. Blasse, *J. Lumin.*, 1997, **72–74**, 129.
14 V. A. Morozov, A. Bertha, K. W. Meert, S. van Rompaey, D. Batuk, G. T. Martinez, S. van Aert, P. F. Smet, M. V. Raskina, D. Poelman, A. M. Abakumov and J. Hadermann, *Chem. Mater.*, 2013, **25**, 4387–4395.
15 C. Sung Lim, *J. Phys. Chem. Solids*, 2015, **78**, 65–69.
16 Y. Liu, Y. Y. Jiang, G. X. Liu, J. X. Wang, X. T. Dong and W. S. Yu, *Chin. J. Inorg. Chem.*, 2013, **2**, 277.
17 S. Han, B. Song, L. Liu, C. He and K. S. Yang, *Chin. J. Lumin.*, 2013, **9**, 1183.
18 Y. Lin, S. K. Gao, G. M. Wang and W. M. Shi, *J. Fuzhou Univ., Nat. Sci. Ed.*, 2008, **1**, 134.

19 V. V. Atuchin, E. N. Galashov, O. Y. Khyzhun, A. S. Kozhukhov, L. D. Pokrovsky and V. N. Shlegel, *Cryst. Growth Des.*, 2011, **11**, 2479–2484.
20 Z. Xia, J. Li, Y. Luo, L. Liao and J. Varela, *J. Am. Ceram. Soc.*, 2012, **95**, 3229–3234.
21 K. R. Kort and S. Banerjee, *Inorg. Chem.*, 2011, **50**, 5539–5544.
22 J. Li, J. Sun, J. Liu, X. Li, J. Zhang, Y. Tian, S. Fu, L. Cheng, H. Zhong, H. Xia and B. Chen, *Mater. Res. Bull.*, 2013, **48**, 2159–2165.
23 M. Sun, L. Ma, B. J. Chen, F. Stepongzi, F. Liu, Z. W. Pan, M. K. Lei and X. J. Wang, *J. Lumin.*, 2014, **152**, 218–221.
24 A. X. S. Bruker, *TOPAS V4 – User's Manual*, Bruker AXS, Karlsruhe, Germany, 2008.
25 M. Pollnau, D. R. Gamelin, S. R. Luthi and H. U. Gudel, *Phys. Rev. B: Condens. Matter Mater. Phys.*, 2000, **61**, 3337.
26 J. Chen, Y.-g. Liu, H. Liu, D. Yang, H. Ding, M. Fang and Z. Huang, *RSC Adv.*, 2014, **4**, 18234.
27 C. Guo, Y. Xu, X. Ding, M. Li, J. Yu, Z. Ren and J. Bai, *J. Alloys Compd.*, 2011, **509**, L38–L41.
28 A. Durairajan, D. Thangaraju, D. Balaji and S. Moorthy Babu, *Opt. Mater.*, 2013, **35**, 740–743.
29 X. Yu, M. Gao, J. Li, L. Duan, N. Cao, Z. Jiang, A. Hao, P. Zhao and J. Fan, *J. Lumin.*, 2014, **154**, 111–115.
30 F. Lei and B. Yan, *J. Solid State Chem.*, 2008, **181**, 855–862.
31 D. H. Templeton and A. Zalkin, *Acta Crystallogr.*, 1963, **16**, 762.
32 V. V. Atuchin, A. S. Aleksandrovsky, O. D. Chimitova, T. A. Gavrilova, A. S. Krylov, M. S. Molokeev, A. S. Oreshonkov, B. G. Bazarov and J. G. Bazarova, *J. Phys. Chem. C*, 2014, **118**, 15404–15411.
33 R. D. Shannon, *Acta Crystallogr., Sect. A: Cryst. Phys., Diffr., Theor. Gen. Crystallogr.*, 1976, **32**, 751.
34 K. Nassau, H. J. Levinstein and G. M. Loiacono, *J. Phys. Chem. Solids*, 1965, **26**, 1805.
35 M. Guan, H. Zheng, L. Mei, M. S. Molokeev, J. Xie, T. Yang, X. Wu, S. Huang, Z. Huang and A. Setlur, *J. Am. Ceram. Soc.*, 2015, **98**, 1182–1187.
36 M. Y. Peng, N. Zhang, L. Wondraczek, J. R. Qiu, Z. M. Yang and Q. Y. Zhang, *Opt. Express*, 2011, **19**, 20799.
37 Y. Wang and J. Ohwaki, *Appl. Phys. Lett.*, 1993, **63**, 3268.
38 P. Du, Z. Xia and L. Liao, *J. Lumin.*, 2013, **133**, 226–229.
39 D. Dai, S. Xu, S. Shi, M. Xie and C. Che, *Opt. Lett.*, 2005, **30**, 3377–3379.
40 J. Zhang, Y. Wang, L. Guo and P. Dong, *Dalton Trans.*, 2013, **42**, 3542–3551.
41 L. Xing, Y. Xu, R. Wang, W. Xu, S. Gu and X. Wu, *Chem. Phys. Lett.*, 2013, **577**, 53–57.
42 J. Zhang, Y. Wang, L. Guo, F. Zhang, Y. Wen, B. Liu and Y. Huang, *J. Solid State Chem.*, 2011, **184**, 2178–2183.
43 H. Yang, S. Xu, C.-H. Tao, V. W.-W. Yam and J. Zhang, *J. Appl. Phys.*, 2011, **110**, 043105.